JOURNAL OF MAGNETIC RESONANCE, Series A 111, 137–149 (1994)

A Flexible Spline Model of the Spin Echo with Applications to Estimation of the Spin–Spin Relaxation Time

JONATHAN RAZ,* THOMAS CHENEVERT,† AND ERIK J. FERNANDEZ‡

*Department of Biostatistics, School of Public Health, University of Michigan, Ann Arbor, Michigan 48109-2029;
†Department of Radiology, School of Medicine, University of Michigan, Ann Arbor, Michigan 48109-0030; and
‡Department of Chemical Engineering, University of Virginia, Charlottesville, Virginia 22903

Received July 6, 1993; revised June 6, 1994

Under weak mathematical assumptions, the distortion due to B_0 inhomogeneity is shown to take the form of a characteristic function, which is the Fourier transform of a probability distribution. A model of the spin echo is proposed that includes a spline approximation to an arbitrary smooth characteristic function. The model is applied to spin echoes acquired from water, water/dioxane, and methanol phantoms, and the fit of the spline model is compared to that of the traditional Lorentzian model. Estimation of the spin–spin relaxation time (T_2) from a single spin-echo data set is demonstrated.

INTRODUCTION

In a perfectly homogeneous magnetic field (B_0), each component of the free-induction decay can be represented by an exponentially decaying complex exponential with decay rate equal to the inverse of the spin–spin relaxation time. In practice, B_0 inhomogeneity and other distortions change the rate and form of the decay, and the true T_2 cannot be recovered from the FID. The standard method for estimating T_2 involves computation of line heights or areas from spin echoes acquired at various echo times. This paper presents a flexible mathematical model of the inhomogeneity distortions in spin-echo signals, with applications to improved estimation of T_2. We point out that T_2 can be estimated from a single spin-echo signal, and we present results on the feasibility of this procedure.

Many authors have suggested fitting NMR signals in the time or frequency domain by an exponential decay (Lorentzian) model with a reduced relaxation time denoted by T_2^* (*1–5*). These models will lead to biased estimates of amplitudes and relaxation times if the true decay is not exponential and the spectral peaks overlap. The HOGWASH (*6*) and QUALITY (*7*) methods convert nonexponential decay to exponential decay under the assumption that all components are distorted by the same multiplicative function. HOGWASH requires an isolated spectral peak, while QUALITY requires a high signal-to-noise ratio (SNR) reference signal with known (or precisely estimated) frequency, phase, and decay rate.

Webb *et al.* (*8*) proposed mapping the B_0 inhomogeneity and using this map to correct observed NMR signals. We propose an alternative approach that does not require the additional scans necessary to map the B_0 field, does not require the spectrometer to have imaging capability, and that includes estimation of T_2 as part of the analysis. Webb *et al.* (*8*) noted limitations of their method in applications to data with short T_2; in general, the performance of our method is improved by short relaxation times.

Instead of trying to eliminate the inhomogeneity distortions, we directly estimate the distortions as part of the model-fitting procedure. We show that under weak mathematical assumptions, these distortions must have a particular form, called a characteristic function. Our model approximates an arbitrary smooth characteristic function using constrained regression splines. Applications to simulated spin echoes and spin echoes acquired from chemical phantoms show that the model separates true T_2 decay from inhomogeneity effects and reduces bias compared to the conventional Lorentzian model.

MATHEMATICAL CONSTRAINTS ON INHOMOGENEITY DISTORTIONS

Let $Y(t_j)$ denote the complex-valued FID at time t_j ($j = 1, \ldots, u$, with the t_j equally spaced), and let $N(t_j)$ denote a complex-valued Gaussian white-noise process. Assume that under B_0 homogeneity, the digitized FID has the form

$$Y(t_j) = \sum_{k=1}^{K} \alpha_k \exp[-\beta_k t_j + i(\omega_k t_j + \phi_k)] + N(t_j), \quad j = 1, \ldots, u, \qquad [1]$$

where α_k is the amplitude of spectral component k, β_k is the decay rate (the inverse of the spin–spin relaxation time), ω_k is the frequency, and ϕ_k is the phase.

1064-1858/94 $6.00

De Graaf *et al.* (7), Webb *et al.* (8), and others assumed that B_0 inhomogeneity has the same effect on every spectral component. Under this assumption we may replace ω_k by $\omega_k + \Delta\omega(\mathbf{r})$, where $\mathbf{r} = (r_1, r_2, r_3)$ is a vector of coordinates in three-dimensional space, and $\Delta\omega(\mathbf{r})$ is the deviation of the true frequency at spatial location $\mathbf{r}$ from the average frequency. Then the FID results from integrating over the entire excited volume (7),

$$Y(t_j) = \psi(t_j) \sum_{k=1}^{K} \alpha_k \exp[-\beta_k t_j + i(\omega_k t_j + \phi_k)] + N(t_j), \quad [2]$$

where, with V denoting the excited volume,

$$\psi(t) = \int_V \exp[i\Delta\omega(\mathbf{r})t]dr_1 dr_2 dr_3. \quad [3]$$

Webb *et al.* (8) proposed measuring a discretized version of $\Delta\omega(\mathbf{r})$ and thus computing an approximation to $\psi(t)$.

Although Eq. [3] seems to suggest that $\psi(t)$ can be any complex-valued function, we show that it must be proportional to a "characteristic function," which is the Fourier transform of a probability-density function (9). A sufficient but not necessary condition for this representation is that $\Delta\omega(\mathbf{r})$ is piecewise constant, that is, that the volume V can be partitioned into an arbitrarily large finite number P of subvolumes V_p of arbitrary shape and size, such that $\Delta\omega(\mathbf{r})$ takes on the constant value ϵ_p for $\mathbf{r} \in V_p$. Let $c = |V| = \int_V dr_1 dr_1 dr_3$ and $c_p = (1/c)|V_p|$. Since $c_p \geq 0$ for $p = 1, \ldots, P$ and $\sum c_p = 1$, we can define a discrete random variable ϵ that takes on value ϵ_p with probability c_p. $\Delta\omega(\mathbf{r})$ is defined to be the deviation from the average value, so that the average of $\Delta\omega(\mathbf{r})$ over the entire volume is zero. This implies that the random variable ϵ has expectation zero,

$$E(\epsilon) = \sum_p \epsilon_p c_p = (1/c) \sum_p \epsilon_p \int_{V_p} dr_1 dr_2 dr_3$$

$$= (1/c) \int_V \Delta\omega(\mathbf{r}) dr_1 dr_2 dr_3 = 0, \quad [4]$$

where $E(\cdot)$ denotes expectation. Furthermore,

$$\psi(t) = \sum_p \int_{V_p} \exp(i\epsilon_p t) dr_1 dr_2 dr_3 = c \sum_p c_p \exp(i\epsilon_p t)$$

$$= c \int_{-\infty}^{\infty} \exp(i\epsilon t) dF(\epsilon), \quad [5]$$

where $F(\epsilon)$ is the cumulative distribution function of the random variable ϵ, and the last integral is the definition of a characteristic function (9).

Although $\Delta\omega(\mathbf{r})$ is assumed piecewise constant, at least some functions $\Delta\omega(\mathbf{r})$ that are not piecewise constant allow $\psi(t)$ to be represented as a characteristic function. We suggest modeling $\psi(t)$ as proportional to the characteristic function of some mean zero probability distribution F without necessarily requiring that F be discrete or that $\Delta\omega(\mathbf{r})$ be piecewise constant.

If $\psi(t)$ is proportional to the characteristic function of a mean zero distribution, then it satisfies the following conditions (9):

1. It is nonnegative definite; that is, for any positive integer n and any real numbers $t_1, \ldots, t_n$, and any complex numbers $\zeta_1, \ldots, \zeta_n$, the sum

$$\sum_{a=1}^{n} \sum_{b=1}^{n} \psi(t_a - t_b)\zeta_a \bar{\zeta}_b \quad [6]$$

is real and nonnegative, where $\bar{\zeta}$ denotes the complex conjugate of ζ. All nonnegative definite functions are Hermitian.

2. The first derivative vanishes at $t = 0$; that is, $\psi'(0) = 0$.

Following are examples of the characteristic-function representation of $\psi(t)$. The constant c is suppressed, since it can be absorbed into the amplitudes α_k in Eq. [2].

Example 1. If F is a *Normal (Gaussian) distribution,* then

$$\psi(t) = \exp(-\gamma t^2), \quad \gamma > 0, \quad [7]$$

leading to a model suggested by Barkhuijsen, de Beer, and van Ormondt (10).

Example 2. If F is a *Cauchy distribution,* then

$$\psi(t) = \exp(-\gamma|t|), \quad \gamma > 0. \quad [8]$$

If we let $\beta_k^* = \beta_k + \gamma$ and $T_{2k}^* = 1/\beta_k^*$, then Eq. [2] with ψ defined by Eq. [8] becomes

$$Y(t_j) = \sum_{k=1}^{K} \alpha_k \exp[-t_j/T_{2k}^* + i(\omega_k t_j + \phi_k)] + N(t_j). \quad [9]$$

Strictly speaking, this example, which is the conventional Lorentzian model, contradicts the assumption that F has mean zero, since the Cauchy distribution does not have a mean.

Example 3. If F is a *stable distribution* (9), which includes the Cauchy and Normal as special cases, then

$$\psi(t) = \exp(-\gamma|t|^{\delta}), \quad \gamma > 0, 0 < \delta \leq 2, \quad [10]$$

which corresponds to a mean zero distribution for $1 < \delta \leq 2$.

Example 4. If F is a mixture of two stable distributions, then

$$\psi(t) = \kappa \exp\{i[(1-\kappa)/\kappa]\nu t - \gamma_1|t|^{\delta_1}\} + (1-\kappa)\exp(i\nu t - \gamma_2|t|^{\delta_2}),$$
$$\gamma_1, \gamma_2 > 0,\ 0 < \delta_1, \delta_2 \leq 2,\ 0 \leq \kappa \leq 1,\ \nu \in \mathbb{R}, \quad [11]$$

where the mixture distribution has mean zero for $1 < \delta_1, \delta_2 \leq 2$.

If $Y(t_j)$ is a spin-echo signal, rather than an FID, then the model defined by Eq. [2] becomes

$$Y(t_j) = \psi(t_j - \tau) \sum_{k=1}^{K} \alpha_k \exp\{-\beta_k t_j + i[\omega_k(t_j - \tau) + \phi_k]\} + N(t_j), \quad [12]$$

where τ is the echo time. Combining Eq. [12] and Eq. [8], the Lorentzian model of the spin echo has the form

$$Y(t_j) = \begin{cases} \exp(\gamma\tau) \sum_{k=1}^{K} \alpha_k \exp[-(\beta_k + \gamma)t_j + i(\omega_k t_j + \phi_k)] + N(t_j), & t_j \geq \tau \\ \exp(-\gamma\tau) \sum_{k=1}^{K} \alpha_k \exp[-(\beta_k - \gamma)t_j + i(\omega_k t_j + \phi_k)] + N(t_j), & t_j < \tau. \end{cases} \quad [13]$$

Thus, T_2^* cannot be defined for a spin echo.

Since ψ is a Hermitian function centered at $t = \tau$, while the true spin–spin relaxation is centered at $t = 0$, it is theoretically possible to estimate the decay rates $\beta_1, \ldots, \beta_K$ from a single spin echo. Short T_2 values (large decay rates) facilitate separation of decay due to spin–spin relaxation from decay due to inhomogeneity, since the asymmetry of the echo is more pronounced when the T_2 is short.

When multiple spin-echo data sets are acquired at distinct echo times, each using a single excitation pulse and single refocusing pulse, we assume a model of the form

$$Y_l(t_{jl}) = \psi(t_{jl} - \tau_l) \sum_{k=1}^{K} \alpha_k \exp\{-\beta_k t_{jl} + i[\omega_k(t_{jl} - \tau_l) + \phi_{kl}]\} + N_l(t_{jl}), \quad l = 1, \ldots, L,\ j = 1, \ldots, u_l, \quad [14]$$

where $Y_l(t_{jl})$ is the complex-valued signal acquired at times t_{jl} $(j = 1, \ldots, u_l)$ in spin-echo data set l, τ_l is the echo time in data set l, ϕ_{kl} is the phase for spectral component k in data set l, $N_l(t)$ is the noise process, and L is the number of spin-echo data sets.

A HERMITIAN SPLINE APPROXIMATION TO A CHARACTERISTIC FUNCTION

The characteristic function representation of ψ suggests a wide range of parametric models, such as the examples in the previous section. However, the functional form of ψ is typically unknown, and it will vary with the spectrometer configuration and the sample characteristics, including the spatial distribution of spins within the bore, the quality of the shim, and the magnetic susceptibility of the object. This suggests that we should develop a flexible and parsimonious representation of an arbitrary characteristic function, insert this representation for ψ in model [12], and fit this model to spin-echo data. Unfortunately, any general model of a characteristic function must be nonlinear or involve inequality constraints or both (*9*). For example, Eq. [11] is fairly flexible, but it is a highly nonlinear function with inequality constraints.

Since fitting Eq. [12] is already a difficult nonlinear optimization problem, we developed a simple approach for approximating $\psi(t)$ by a regression spline (*11*) that is constrained, like the characteristic function of a mean zero distribution, to be Hermitian and to have a derivative that vanishes at $t = 0$. The spline is linear in the unknown regression coefficients, and it is a smooth function of time. The smoothness helps exclude noise effects, since under the assumption of Gaussian white noise, the noise process is inherently rough. The disadvantage of the spline function is that it satisfies only the Hermitian condition and not necessarily the stricter nonnegative definite constraint, so that the spline model is less parsimonious than a model that takes advantage of the stricter constraint.

Regression splines are defined by a set of functions that form a basis for the space of piecewise polynomials satisfying certain continuity constraints at the join points ("knots") (*11*). One standard form of a regression spline, which is easily modified to satisfy the Hermitian and zero derivative constraints, is defined by the "+"-function basis,

$$g(t) = \sum_{m=0}^{q} \lambda_m t^m + \sum_{m=1}^{s} \lambda_{q+m}(t - \xi_m)_+^q, \quad [15]$$

where the positive integer q is the order of the spline, $\lambda_0, \ldots, \lambda_{q+s}$ are regression coefficients, the knots $\xi_1, \ldots, \xi_s$ are specified real constants satisfying $\xi_1 < \cdots < \xi_s$, and the +-function is defined by $(t)_+^q = t^q$, $t \geq 0$; $(t)_+^q = 0$, $t < 0$. The function g has $q - 1$ continuous derivatives with respect to t and the regression coefficients.

A real-valued spline g_0 that is constrained to be an even function can be obtained from

$$g_0(t) = \sum_{m=0}^{q} \lambda_{2m} t^{2m} + \sum_{m=1}^{s} \lambda_{2q+2m}(|t| - \xi_m)_+^{2q}, \quad [16]$$

where q is a positive integer and $\lambda_0, \lambda_2, \ldots, \lambda_{2q+2s}$ are regression coefficients. Regardless of the values of the regression coefficients, $g_0'(0) = 0$. A real-valued spline g_1 that is constrained to be an odd function and to have derivative zero at $t = 0$ can be obtained from

$$g_1(t) = \sum_{m=2}^{q} \lambda_{2m-1} t^{2m-1} + \operatorname{sgn}(t) \sum_{m=1}^{s} \lambda_{2q+2m-1} (|t| - \xi_m)_+^{2q-1}, \quad [17]$$

where $\lambda_3, \lambda_5, \ldots, \lambda_{2q+2s-1}$ are regression coefficients.

Let $\boldsymbol{\eta}_1 = (\lambda_0, \lambda_2, \lambda_3, \lambda_4, \ldots, \lambda_{2q+2s})^T$ be the $(2q + 2s) \times 1$ vector of parameters needed to define both an even and an odd spline (where T denotes transpose), so that $h(t; \boldsymbol{\eta}_1) = g_0(t) + ig_1(t)$ is a smooth Hermitian function that is linear in the $2q + 2s$ regression parameters. Note that we force the derivative of h at zero to be zero simply by excluding the $m = 1$ term in the first sum of Eq. [17]. We fix $q = 2$, so that $h(t; \boldsymbol{\eta}_1)$ has at least two continuous derivatives at every value of t. Choice of the number of knots s and the knot positions $\xi_1, \ldots, \xi_s$ is discussed below. We refer to model [12] or model [14] with $\psi(t)$ defined to be the Hermitian spline function $h(t; \boldsymbol{\eta}_1)$ as the Hermitian spline model of the spin echo.

MAXIMUM-LIKELIHOOD ESTIMATION OF MODEL PARAMETERS

Given known values of the echo time τ and the knots $\xi_1, \ldots, \xi_s$, the Hermitian spline model is a fully specified parametric model in terms of the spline parameter vector $\boldsymbol{\eta}_1$ and the NMR parameter vector $\boldsymbol{\eta}_2 = (\alpha_2, \ldots, \alpha_K, \beta_1, \ldots, \beta_K, \omega_1, \ldots, \omega_K, \phi_1, \ldots, \phi_K)^T$. For identifiability of the model, we set α_1 to be a constant equal to one, and we deliberately omit α_1 from the vector of unknown parameters $\boldsymbol{\eta}_2$. Under the assumption that the noise process $N(t_j)$ is Gaussian white noise, the maximum-likelihood estimators are the values that minimize the objective function

$$O(\boldsymbol{\eta}_1, \boldsymbol{\eta}_2) = \sum_{j=1}^{u} |Y(t_j) - \mu_j(\boldsymbol{\eta}_1, \boldsymbol{\eta}_2)|^2, \quad [18]$$

where

$$\mu_j(\boldsymbol{\eta}_1, \boldsymbol{\eta}_2) = h(t_j - \tau; \boldsymbol{\eta}_1) \sum_{k=1}^{K} \alpha_k \exp\{-\beta_k t_j + i[\omega_k(t_j - \tau) + \phi_k]\}. \quad [19]$$

We minimized $O(\boldsymbol{\eta}_1, \boldsymbol{\eta}_2)$ by a modification of the Levenberg–Marquardt algorithm that exploits the linear structure of the spline function. The algorithm is closely related to the variable projection algorithm (*2, 3, 12*) and other algorithms described in (*12*).

Let $\mathbf{y} = [Y(t_1), \ldots, Y(t_u)]^T$ and $\boldsymbol{\mu}(\boldsymbol{\eta}_1, \boldsymbol{\eta}_2) = [\mu_1(\boldsymbol{\eta}_1, \boldsymbol{\eta}_2), \ldots, \mu_u(\boldsymbol{\eta}_1, \boldsymbol{\eta}_2)]^T$. Note that $\boldsymbol{\mu}(\boldsymbol{\eta}_1, \boldsymbol{\eta}_2) = \mathbf{X}\boldsymbol{\eta}_1$, where $\mathbf{X}$ is a $u \times (2q + 2s)$ matrix with element (j, m) equal to the product of $\sum_{k=1}^{K} \alpha_k \exp\{-\beta_k t_j + i[\omega_k(t_j - \tau) + \phi_k]\}$ and the mth of the values

$$1, (t_j - \tau)^2, i(t_j - \tau)^3, (t_j - \tau)^4, i \operatorname{sgn}(t_j - \tau)(|t_j - \tau| - \xi_1)_+^3, (|t_j - \tau| - \xi_1)_+^4, \ldots, i \operatorname{sgn}(t_j - \tau)(|t_j - \tau| - \xi_s)_+^3, (|t_j - \tau| - \xi_s)_+^4. \quad [20]$$

Thus, the least-squares estimate of $\boldsymbol{\eta}_1$, given a fixed value of $\boldsymbol{\eta}_2$, is

$$\hat{\boldsymbol{\eta}}_1 = (\bar{\mathbf{X}}^T\mathbf{X})^{-1}\bar{\mathbf{X}}^T\mathbf{y}. \quad [21]$$

Let $\boldsymbol{\eta} = (\boldsymbol{\eta}_1^T, \boldsymbol{\eta}_2^T)^T$ and $\mathbf{D} = \partial\boldsymbol{\mu}/\partial\boldsymbol{\eta}^T$. The modified Levenberg–Marquardt algorithm is defined by the following steps.

Step 1. Set $n = 0$. Set the Levenberg–Marquardt parameter w to a some small starting value. Compute starting values $\boldsymbol{\eta}_2^{(n)}$. Compute starting values $\boldsymbol{\eta}_1^{(n)}$ using Eq. [21] with $\boldsymbol{\eta}_2^{(n)}$ substituted for $\boldsymbol{\eta}_2$ in the definition of $\mathbf{X}$. Compute $O[\boldsymbol{\eta}_1^{(n)}, \boldsymbol{\eta}_2^{(n)}]$.

Step 2. Compute the matrix $\mathbf{D}$ evaluated at $\boldsymbol{\eta} = [(\boldsymbol{\eta}_1^{(n)})^T, (\boldsymbol{\eta}_2^{(n)})^T]^T$, and the update vector

$$\boldsymbol{\delta} = (\bar{\mathbf{D}}^T\mathbf{D} + w\mathbf{I})^{-1}\bar{\mathbf{D}}^T[\mathbf{y} - \boldsymbol{\mu}(\boldsymbol{\eta}_1^{(n)}, \boldsymbol{\eta}_2^{(n)})], \quad [22]$$

where $\mathbf{I}$ is the identity matrix. Compute $\boldsymbol{\eta}_2^{(n+1)} = \boldsymbol{\eta}_2^{(n)} + \boldsymbol{\delta}_2$, where $\boldsymbol{\delta}_2$ is the subvector of $\boldsymbol{\delta}$ corresponding to $\boldsymbol{\eta}_2$.

Step 3. Compute $\boldsymbol{\eta}_1^{(n+1)}$ using Eq. [21] with $\boldsymbol{\eta}_2^{(n+1)}$ substituted for $\boldsymbol{\eta}_2$ in the definition of $\mathbf{X}$.

Step 4. Compute the objective function $O[\boldsymbol{\eta}_1^{(n+1)}, \boldsymbol{\eta}_2^{(n+1)}]$. If the objective function has decreased by only a negligible amount, stop. Otherwise, if the objective function has increased, substitute $10w$ for w and go to Step 2; if the objective function has decreased, substitute $w/10$ for w, increment n, and go to Step 2.

In the actual implementation, the computations of $\boldsymbol{\delta}$ and $\boldsymbol{\eta}_1^{(n)}$ are performed using a numerically stable least-squares algorithm.

We also implemented an algorithm that fits the Lorentzian model [*13*] to a time-domain spin-echo signal. This algorithm is the same as the algorithm for the Hermitian spline model, except that Step 3 and all references to $\boldsymbol{\eta}_1$ are omitted, and $\boldsymbol{\eta}_2$ is defined to include α_1 and the parameter γ that appears in Eq. [8].

We generalized these algorithms in order to fit model [14] to multiple spin-echo data sets acquired at distinct echo times. The fitting algorithm was the same as that described

for single-echo data sets, except that separate phase parameters ϕ_{kl} were estimated for each echo.

DETAILS OF THE MODEL AND ALGORITHMS

Based on applications to simulated and real data, we recommend that the number of knots s be 3, 4, 5, or 6, since the NMR parameter estimates can be extremely biased when $s < 3$ and highly unstable when $s > 6$. The number and placement of knots can be selected using the Akaiki information criterion (AIC), the Bayesian–Schwartz criterion (SBC), or the Hannan–Quinn criterion (HQC) (*13–15*), which attempt to balance maximization of the likelihood against minimization of the number of model parameters. For related applications of these methods, see (*16, 17*). As described below, all three criteria performed well in applications to simulated data.

The model-selection criteria also could be used to choose the location of the knots, but this procedure would require refitting the model with many different sets of knot locations. As an alternative, we suggest a generally applicable formula for knot placement. Since the time points are equally spaced, it might seem natural to use equally spaced knots in defining the spline function. A better approach is to equally space the knots on a logarithmic scale, under the assumption that $\psi(t)$ exhibits roughly exponential changes, which leads to the definition

$$\xi_m = \exp\{\log[(t_u - t_1)/2 + 1]m/(s + 1)\} - 1, \quad m = 1, \ldots, s. \qquad [23]$$

In applications to real data sets with high SNR, logarithmic knot placement consistently yielded better fits than did linear placement of the knots.

The set of spline basis vectors defined by expression [20] evaluated at $j = 1, \ldots, u$ are highly collinear. One alternative would be to use the B-spline basis (*11*), but we prefer the intuitive simplicity of the even and odd splines when expressed in the +-function basis. To avoid numerical problems, we applied the modified Gram–Schmidt algorithm (*18*) to the basis vectors before computation of the maximum-likelihood estimators. Thus, the matrix **X** was computed in terms of orthogonalized spline vectors, as were the various quantities computed in Step 2 of the modified Levenberg–Marquardt algorithm. The orthogonalization has no effect on the interpretation of the NMR parameter estimates.

Starting values for the frequencies $\omega_1, \ldots, \omega_K$ were the peak frequencies in the magnitude spectrum (modulus of the Fourier transform of the data). Starting values for the phase parameters $\phi_1, \ldots, \phi_K$ were computed from the argument of the complex demodulate (*19*) of the data at the peak frequencies. For $k = 1, \ldots, K$, a starting value for the decay parameter β_k was obtained by a weighted least-squares fit of $-\beta_k t - \gamma|t - \tau|$ to the logarithm of the magnitude of the kth demodulate. We defined a preliminary estimate of $\psi(t)$ to be equal to $\exp(-\gamma|t - \tau|)$ for the estimate of γ computed from the demodulate of the highest peak, and then computed starting values for the amplitude parameters $\alpha_1, \ldots, \alpha_K$ by ordinary least squares (*1–3*). As described in the previous section, a refined estimate of $\psi(t)$ was computed using Eq. [21] before the first Levenberg–Marquardt iteration. When fitting the Hermitian spline model to multiple spin-echo data sets, we obtained starting values for the decay parameters β_k from the peak heights of the Fourier transforms of the signals.

In the fitting of model [12] to a single spin echo, very small changes in the value of τ can lead to large changes in the estimates of the decay times $T_{2k} = 1/\beta_k$, but estimating τ in the modified Levenberg–Marquardt procedure complicates estimation of the spline coefficients and can lead to numerical instability. As an alternative, a nearly correct value of τ was computed from the exact timing of the pulse sequence, and then improved by fitting model [12] to each value in a grid around this preliminary estimate and choosing the fit that minimized the objective function.

APPLICATION TO PHANTOM DATA

We compared the fit of the Hermitian spline model to that of the Lorentzian model in applications to proton spin echoes acquired from six different chemical phantoms: distilled water with a 50, 100, or 200 micromolar (μM) concentration of manganese chloride ($MnCl_2$) in solution; dioxane ($C_4H_8O_2$) mixed with a solution of 50 or 100 μM $MnCl_2$ in distilled water; and pure methanol (CH_3OH). These phantoms are designated W5, W10, W20, D5, D10, and MeOH; echoes acquired from W5, W10, and W20 have one spectral component ($K = 1$), while echoes acquired from D5, D10, and MeOH have two components ($K = 2$). The W and D sets of water/manganese solutions were prepared at different times, so that two phantoms with the same nominal molar concentrations of manganese probably had slightly different true concentrations.

Spin echoes were acquired on a 2 T/31 cm Omega CSI spectrometer (Bruker Instruments; formerly GE NMR Instruments, Fremont, California), using a 14 cm birdcage-design transmit and receive RF coil. The pulse sequence was a 90°–180° acquisition of $u = 1024$ time points digitized at 40,000 Hz (for the W5 phantom) and 20,000 Hz (for the other five phantoms). Single-echo spin echoes were acquired at nominal echo times $\tau = 50$, 100, 200 ms (for the W5 phantom) or $\tau = 50$, 100, 200, 300 ms (for the other five phantoms). All acquisitions were performed with only partial optimization of the shimming, so that considerable inhomogeneity was present. The signals were averages of 32 phase-cycled (*20*) acquisitions following eight dummy scans, giving spin echoes with very high SNR. The phase cycling is essential

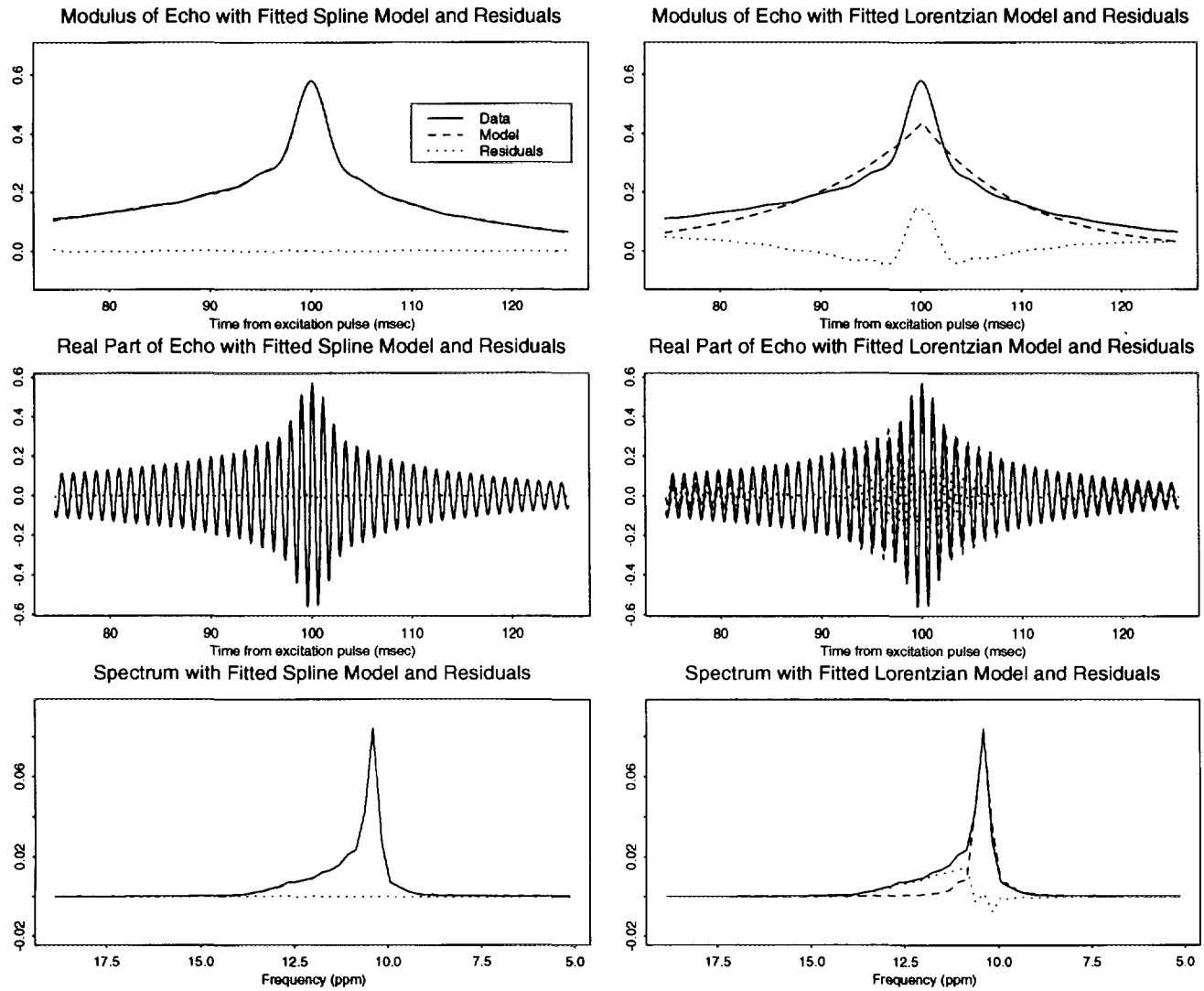

FIG. 1. Comparison of fitted spline and Lorentzian models with spin-echo data acquired from a phantom containing a 100 μM solution of $MnCl_2$ in distilled water. The modulus and real part of the time-domain data and fitted models are displayed, as well as the modulus of the Fourier transforms. In all plots, the solid line indicates the data, the dashed line the model, and the dotted line the difference between the data and the model (residual). The spline model nearly interpolates the data, while the Lorentzian model exhibits serious bias. The Hermitian spline function had six knots equally spaced on a logarithmic scale.

for estimation of T_2 from a single spin echo, since the effects of an imperfect refocusing pulse can obscure the subtle T_2 effects.

We selected six knots ($s = 6$) for the Hermitian spline model, because fewer than six produced noticeably poorer fits to the data, while more led to only small improvements in goodness of fit and resulted in only small changes in the estimates of the NMR parameters.

We fitted the Hermitian spline and Lorentzian models to each of the spin echoes using values of τ that were -0.12, $-0.10, \ldots, 0, \ldots, 0.10, 0.12$ ms from the τ computed using the known timing of the acquisitions. For each model, the value that minimized the objective function was used as the "true" τ.

Multiecho T_2 estimates for use as "gold standards" were computed by fitting model [14] to multiple spin-echo data sets comprising signals acquired at all available values of τ (three values for the W5 phantom, and four for the other five phantoms).

Figures 1, 2, and 3 compare the fitted model to the time-domain signal and to the Fourier transform of three selected spin echoes. Results for the other echoes are qualitatively similar. The spline fit seems nearly perfect, while the Lorentzian model shows noticeable departures from the data. To quantify the fit of the models, we computed the residual sum of squares, which is the objective function (Eq. [18]) evaluated at the maximum-likelihood estimates, and we expressed the residual sum of squares as a percentage of the

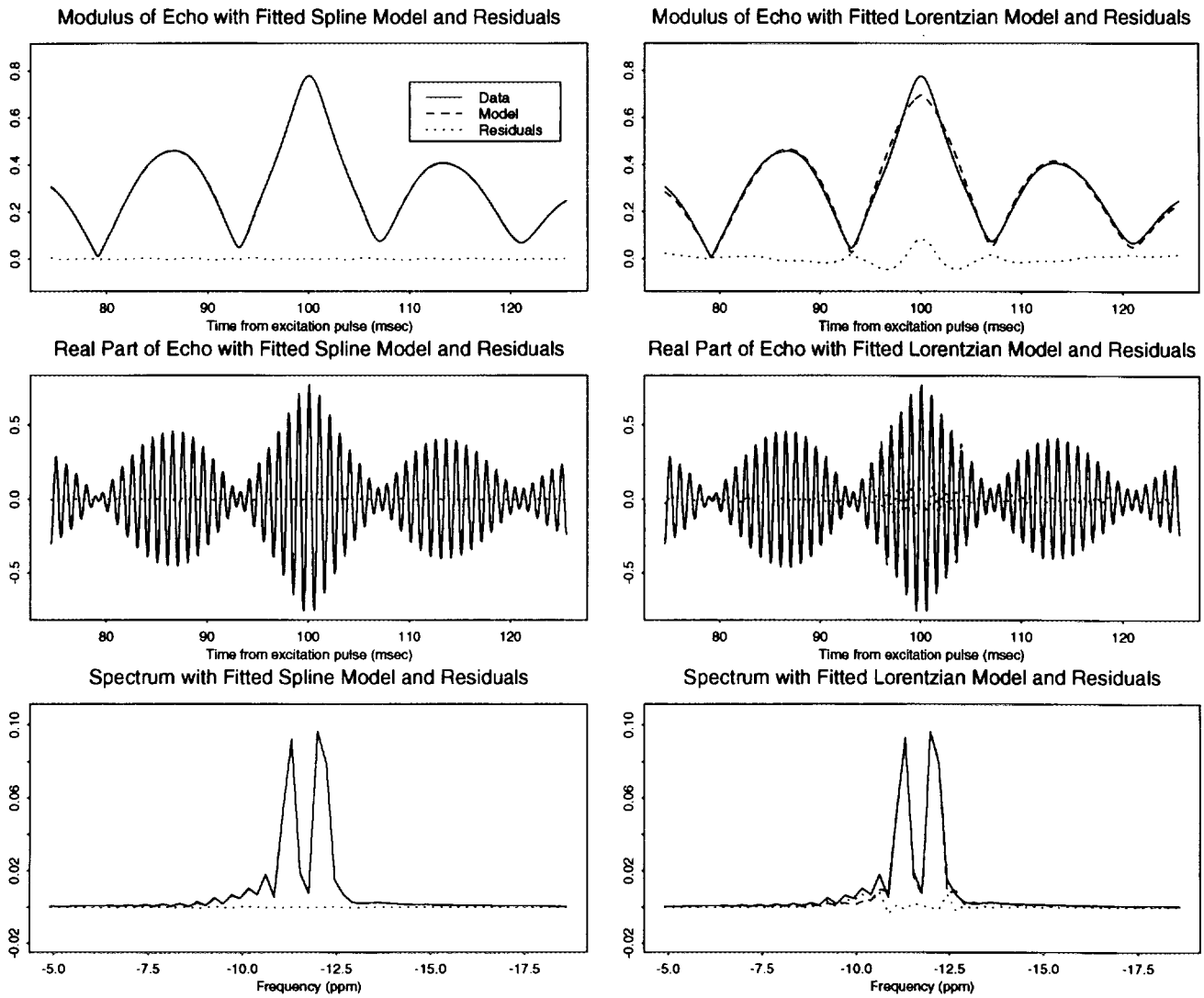

FIG. 2. Comparison of fitted spline and Lorentzian models with echo acquired from a phantom containing dioxane mixed with a 100 μM solution of $MnCl_2$ in distilled water.

total sum of squares $\sum_{j=1}^{\mu} |Y(t_j)|^2$. For the spline fits, the median of this measure was 0.012% with a range of 0.0015 to 0.070%, while for Lorentzian fits, the median was 9.1% with a range of 1.3 to 13.3%.

Table 1 shows the estimated T_2 values (computed as the reciprocal of the estimated β_1 values) of the W20, W10, and W5 phantoms. The multiecho estimates based on the two models are nearly the same. The Hermitian spline single-echo estimates are consistently within 10% of the multiecho estimates, while the Lorentzian estimates are within 20%. The error in the single-echo estimates increases with the relaxation time, apparently because the single-echo estimates are based on small departures from symmetry, and the symmetry of the echo increases with the T_2.

Based on estimated standard errors computed from the Cramer–Rao lower bound (which should approximately hold for these maximum-likelihood estimators), and on the results of the simulation study, we conclude that much of the error in the single-echo T_2 estimates can not be explained by the noise in the data. Some of the error may be due to artifacts caused by imperfections in the refocusing pulse that were not removed by phase cycling, and possibly by diffusion during the acquisition period. A more sophisticated version of the spline model might be able to adjust for these artifacts. In the case of the Lorentzian model, serious misspecification of the function ψ also seems to contribute to the error.

Table 2 shows the estimated T_2 values of the D10, D5, and MeOH phantoms. For the D10 and D5 phantoms, the T_2 estimates are given for water first and then dioxane, while for the MeOH phantom, the estimates are given for hydroxyl and then methyl. The multiecho estimates for the two models disagree, indicating that the form of the inhomogeneity

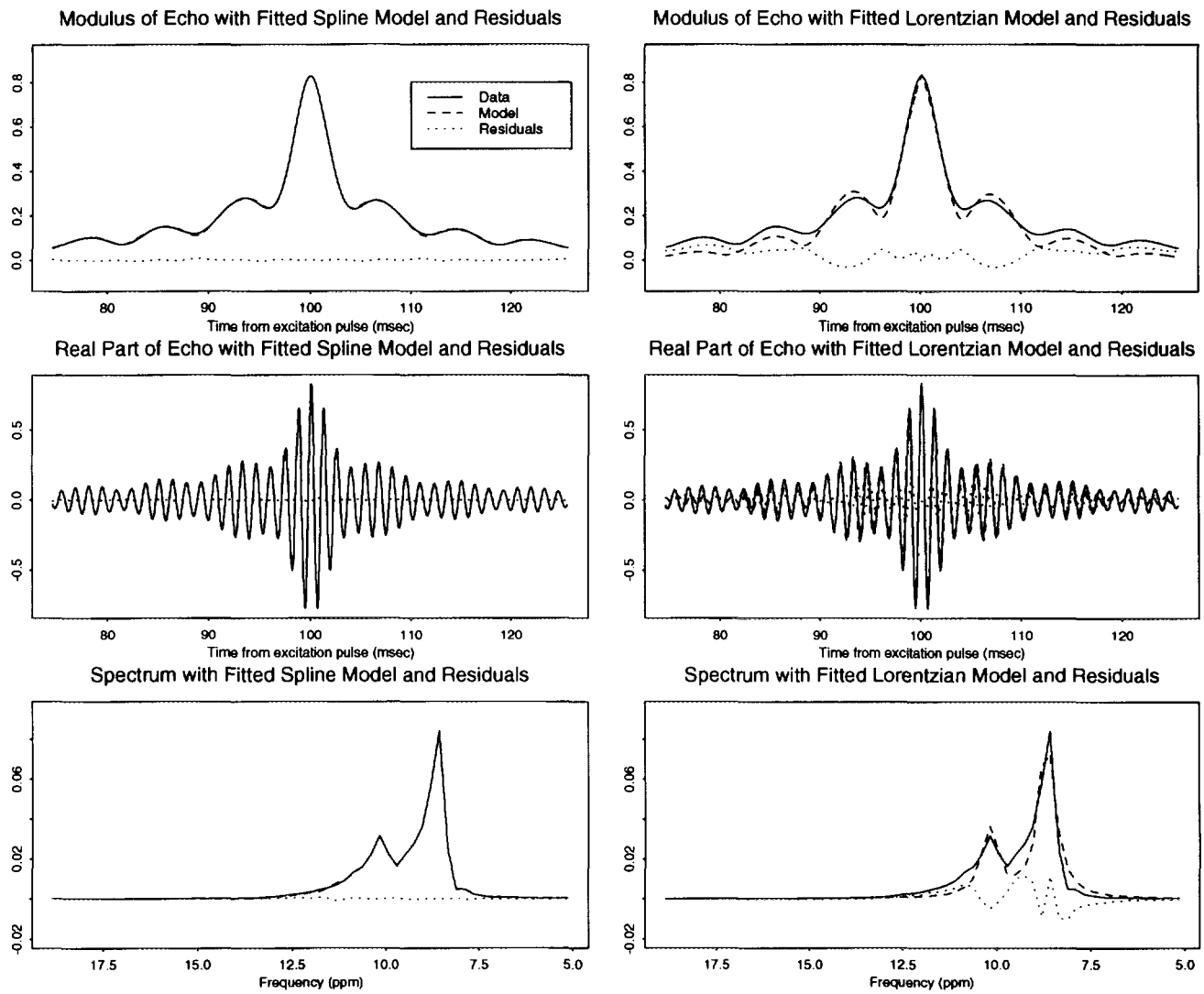

FIG. 3. Comparison of fitted spline and Lorentzian models with echo acquired from a phantom containing methanol.

model is important for correct separation of spectral components. Since the fit of the Hermitian spline model is much better, we expect that the spline T_2 estimates are closer to the true relaxation times.

The single-echo estimates of the long dioxane relaxation time, particularly the spline estimates, are surprisingly good, while both models give erroneous single-echo estimates of T_2 for MeOH. Analysis of simulated data that was designed to resemble the $\tau = 100$ MeOH signals produced much smaller errors, indicating that the errors in the analysis of the phantom may be due to the type of data artifacts discussed above. The relative magnitude of the Lorentzian estimates computed from the $\tau = 100$ MeOH echo does not even reflect the correct ordering of the T_2 values, against suggesting that the Lorentzian model is not able to correctly separate decay due to the two spectral components. The spline single-echo estimates are correctly ordered, but they are considerably greater than the multiecho estimates, except for the $\tau = 300$ echo.

To quantify the agreement between the single-echo and the multiecho T_2 estimates, we computed a statistic defined by

$$\rho = \left[1 + \frac{\sum_{a=1}^{A} (x_a - y_a)^2}{\sum_{a=1}^{A} (x_a - x_\cdot)^2}\right]^{-1}, \qquad [24]$$

where $x_1, \ldots, x_A$ are the logarithms of the multiecho gold-standard T_2 estimates, $x_\cdot = (1/A) \sum x_a$, and $y_1, \ldots, y_A$ are the logarithms of the single-echo estimates. The statistic ρ is zero when there is no agreement and one when there is perfect agreement; this form of ρ was recently proposed by Roy St. Laurent (personal communication) and is similar to the "concordance correlation coefficient" of Lin (*21*). When ρ is computed from the logarithms of the T_2 estimates, it is

TABLE 1

Estimated Spin–Spin Relaxation Time (in Milliseconds) of Protons in Three Water Phantoms for Two Inhomogeneity Models[a]

Phantom	τ	Inhomogeneity model: Lorentz	Inhomogeneity model: Spline
W20	All	*55*	*55*
	50	51	55
	100	51	55
	200	51	55
W10	All	*94*	*94*
	50	78	97
	100	77	96
	200	79	98
	300	85	98
W5	All	*198*	*196*
	50	172	212
	100	167	214
	200	171	212
	300	184	215

[a] In the column headed τ, the numerical values are for the single-echo estimates, while "All" indicates the gold-standard estimates based on all available echoes. These gold-standard estimates are italicized.

identical to ρ computed from the logarithms of the β_k estimates.

Based on the logarithms of the estimates in Tables 1 and 2, $\rho \geq 0.97$ for the single-echo Hermitian spline model using either the spline or Lorentzian multiecho estimates as the gold standard, $\rho = 0.95$ for the single-echo Lorentzian model using the Lorentzian multiecho gold standard, but $\rho = 0.89$ for the single-echo Lorentzian model using the spline multiecho gold standard. Thus, if we believe that the spline multiecho estimates are closer to the true relaxation times, then the spline single-echo estimates are a substantial improvement over the Lorentzian estimates. This conclusion is substantiated by the simulation study.

APPLICATIONS TO COMPUTER-SIMULATED DATA

Simulated spin-echo data were generated to further compare the Lorentzian and Hermitian spline models, to investigate the effects of noise on the single-echo decay rate and amplitude estimates, and to evaluate the model-selection criteria. While the Hermitian spline model gives a much better fit to the real data, it requires many additional parameters, making it more susceptible to noise effects. We expected that the Hermitian spline model would lead to lower bias of the amplitude and decay-rate estimators, while the Lorentzian model would lead to lower variance, so that the mean-square error (squared bias plus variance) would favor the Hermitian spline model at high SNRs and the Lorentzian model at low SNRs.

We simulated a spin echo by generating a signal from Eq. [12], with $N(t_j)$ representing pseudo-random complex-valued Gaussian white noise. The parameters α_k, β_k, ω_k, and ϕ_k were set equal to the estimates of these parameters obtained from (i) the $\tau = 100$ spin echo acquired from the MeOH phantom and (ii) the $\tau = 100$ spin echo acquired from the D10 phantom. The actual parameter values are given in the notes to Tables 3 and 4; the MeOH data contain spectral components with decay rates that differ by a factor of 2, while the D10 data contain spectral components with decay rates that differ by more than an order of magnitude. The simulated function ψ was defined by Eq. [11], with $\kappa = 0.6$, $\nu = 0.12$, $\gamma_1 = 0.013$, $\gamma_2 = 0.15$, $\delta_1 = \delta_2 = 1.5$, which give a spectral peak that is intermediate between a Gaussian and Lorentzian, but somewhat asymmetrical. This particular function was chosen because it qualitatively resembles the ψ functions estimated from the real data and because this simulated ψ does not conform perfectly to either the Lorentzian or the Hermitian spline models.

The signal amplitude was defined to be equal to the maximum magnitude of the simulated time-domain signal in the absence of noise, the noise amplitude to be the standard deviation of the complex-valued simulated white noise, and the SNR to be the ratio of these amplitudes.

TABLE 2

Estimated Spin–Spin Relaxation Time (in Milliseconds) of Protons in Two Water/Dioxane Phantoms and the Methanol Phantom for Two Inhomogeneity Models[a]

Phantom	τ	Inhomogeneity model: Lorentz	Inhomogeneity model: Spline
D10	All	*118, 2087*	*107, 1765*
	50	117, 3157	111, 1706
	100	115, 2017	108, 1634
	200	138, 2795	101, 1954
	300	195, 2550	110, 2153
D5	All	*200, 2193*	*188, 1826*
	50	209, 4734	195, 2022
	100	191, 1891	190, 1568
	200	217, 2429	203, 2231
	300	215, 3520	183, 3201
MeOH	All	*184, 382*	*123, 370*
	50	252, 466	208, 598
	100	351, 305	208, 451
	200	270, 273	162, 423
	300	254, 297	124, 414

[a] In the column headed τ, the numerical values are for the single-echo estimates, while "All" indicates the gold-standard estimates based on all available echoes. These gold-standard estimates are italicized. For the D10 and D5 phantoms, the first estimate in each pair corresponds to the water component, and the second to the dioxane component. For the MeOH phantom, the first estimate corresponds to the hydroxyl component, and the second to the methyl component.

TABLE 3

Results of Simulation Study Based on Methanol Data: Estimated Root-Mean-Square Error of Estimators (as Percentage of True Parameter Value) of Amplitudes (α_k) and Decay Rates (β_k) for Each Signal-to-Noise Ratio (SNR) and Inhomogeneity Model

		Inhomogeneity model			
SNR	Estimator	Spline, 2 knots	Spline, 4 knots	Spline, 6 knots	Lorentz
∞	$\hat{\alpha}_1$	5.5	0.8	0.6	1.1
	$\hat{\alpha}_2$	7.5	1.1	0.5	3.3
	$\hat{\beta}_1$	18.3	0.1	0.2	15.9
	$\hat{\beta}_2$	2.1	0.0	0.0	8.7
100	$\hat{\alpha}_1$	5.8	2.7	2.7	2.4
	$\hat{\alpha}_2$	7.7	1.4	1.0	3.5
	$\hat{\beta}_1$	18.7	5.6	5.5	16.3
	$\hat{\beta}_2$	4.3	3.8	3.8	9.5
30	$\hat{\alpha}_1$	7.9	9.2	9.4	7.7
	$\hat{\alpha}_2$	8.0	3.4	3.3	4.7
	$\hat{\beta}_1$	21.4	19.0	19.0	20.4
	$\hat{\beta}_2$	14.3	13.8	13.9	17.5
10	$\hat{\alpha}_1$	21.8	23.9	28.6	20.1
	$\hat{\alpha}_2$	10.8	8.1	8.9	9.1
	$\hat{\beta}_1$	69.9	50.8	[a]	47.2
	$\hat{\beta}_2$	26.2	35.5	35.6	38.8
2	$\hat{\alpha}_1$	[a]	[a]	[a]	[a]
	$\hat{\alpha}_2$	57.7	70.4	68.9	86.2
	$\hat{\beta}_1$	[a]	[a]	[a]	[a]
	$\hat{\beta}_2$	[a]	[a]	[a]	[a]

Note. The true parameter values used to generate the simulated data were set equal to the estimates obtained from the spline analysis of the $\tau = 100$ echo acquired from the methanol phantom. The true parameters are $\alpha_1 = 0.2981$, $\alpha_2 = 0.8054$, $\beta_1 = 0.004802$ ms^{-1}, $\beta_2 = 0.002216$ ms^{-1}, $\omega_1 = 5.7301$ rad/ms = 10.666 ppm, $\omega_2 = 4.8889$ rad/ms = 9.100 ppm, $\phi_1 = 0.03502$ rad, $\phi_2 = 0.03992$ rad. The amplitudes are in arbitrary units depending on the scaling of the spline function used to estimate $\psi(t)$.

[a] RMSE exceeded 100% of true parameter value.

To compare the spline and Lorentzian models and to evaluate the effects of the SNR on the amplitude and decay-rate estimates, we simulated data at five SNRs: ∞ (no noise), 100, 30, 10, and 2. Figure 4 shows the spectrum of the infinite SNR simulated spin echo and a typical simulated spin echo at the lowest SNR. For each of the two parameter sets (that is, the parameters obtained from the analyses of the real MeOH and D10 phantoms) and each of the four finite SNRs, 100 data sets were simulated and each data set was analyzed using the Lorentzian model and the Hermitian spline model with $s = 2$, 4, and 6 knots.

We estimated the root-mean-square error (RMSE) of the estimators of α_k and β_k for $k = 1, 2$. When the SNR is infinite, the RMSE is simply the absolute bias, since the variance is zero, while the estimated RMSE for the finite SNR simulations is the square root of the mean of squared differences between estimated and true parameters. Table 3 gives the estimated RMSE as a percentage of the true parameter value for the simulations based on the analysis of the MeOH data, and Table 4 gives the results for the simulations based on the analysis of the D10 data.

As indicated by the RMSE for the SNR = ∞ simulations, the 4- and 6-knot Hermitian spline models lead to very little bias, while the Lorentzian model gives seriously biased estimates, except for α_1 in the simulated methanol data. The Hermitian spline model appears to give good estimates of

TABLE 4

Results of Simulation Study Based on Water/Dioxane Data: Estimated Root-Mean-Square Error of Estimators (as Percentage of True Parameter Value) of Amplitudes (α_k) and Decay Rates (β_k) for Each Signal-to-Noise Ratio (SNR) and Inhomogeneity Model

		Inhomogeneity model			
SNR	Estimator	Spline, 2 knots	Spline, 4 knots	Spline, 6 knots	Lorentz
∞	$\hat{\alpha}_1$	5.4	1.0	0.5	5.2
	$\hat{\alpha}_2$	1.4	1.0	0.6	6.5
	$\hat{\beta}_1$	5.9	0.2	0.1	11.3
	$\hat{\beta}_2$	17.6	0.1	0.1	14.3
100	$\hat{\alpha}_1$	5.6	1.6	1.4	5.4
	$\hat{\alpha}_2$	1.8	1.5	1.3	6.5
	$\hat{\beta}_1$	6.2	1.4	1.4	11.3
	$\hat{\beta}_2$	27.4	20.3	20.6	27.6
30	$\hat{\alpha}_1$	7.1	4.9	4.9	6.8
	$\hat{\alpha}_2$	4.7	4.5	4.3	8.2
	$\hat{\beta}_1$	8.2	5.3	5.3	11.8
	$\hat{\beta}_2$	69.7	69.7	69.6	76.2
10	$\hat{\alpha}_1$	13.5	13.5	26.0	11.5
	$\hat{\alpha}_2$	12.3	12.4	[a]	14.6
	$\hat{\beta}_1$	16.8	14.4	20.4	14.6
	$\hat{\beta}_2$	[a]	[a]	[a]	[a]
2	$\hat{\alpha}_1$	[a]	[a]	[a]	[a]
	$\hat{\alpha}_2$	[a]	[a]	[a]	84.5
	$\hat{\beta}_1$	94.8	85.9	81.6	76.8
	$\hat{\beta}_2$	[a]	[a]	[a]	[a]

Note. The true parameter values used to generate the simulated data were set equal to the estimates obtained from the spline analysis of the $\tau = 100$ echo acquired from the D10 phantom. The true parameters are $\alpha_1 = 0.8607$, $\alpha_2 = 0.465$, $\beta_1 = 0.009277$ ms^{-1}, $\beta_2 = 0.0006119$ ms^{-1}, $\omega_1 = -5.8742$ rad/ms = -10.935 ppm, $\omega_2 = -6.3240$ rad/ms = -11.772 ppm, $\phi_1 = 0.08708$ rad, $\phi_2 = 0.09189$ rad. The amplitudes are in arbitrary units depending on the scaling of the spline function used to estimate $\psi(t)$.

[a] RMSE exceeded 100% of true parameter value.

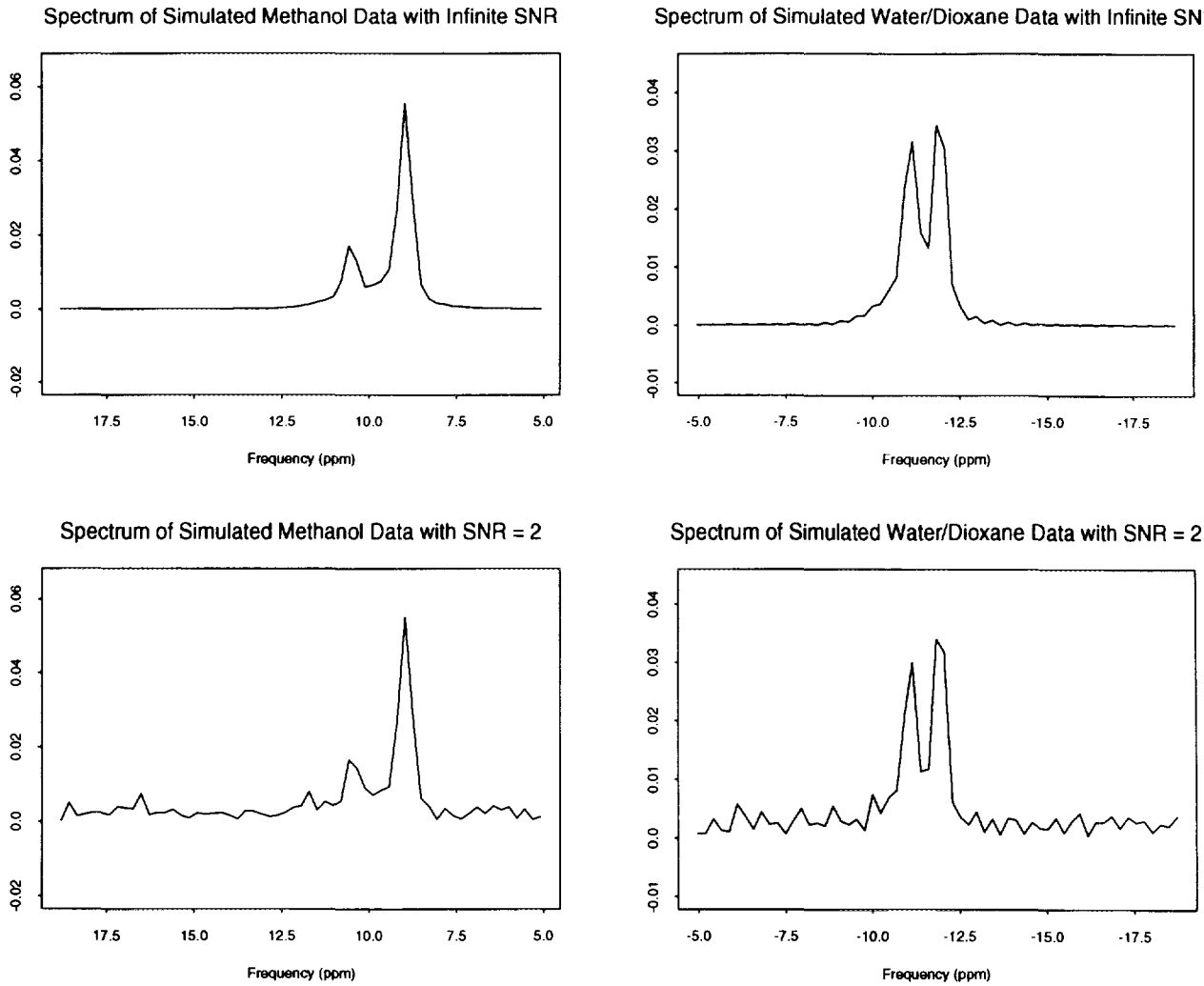

FIG. 4. Spectra (moduli of Fourier transforms) of simulated spin echoes with infinite SNR and with SNR = 2, where SNR is defined as the maximum amplitude of the modulus of the time-domain signal divided by the noise standard deviation.

T_2 from a single echo when the SNR is 30 or above, although the errors can be large for long T_2 values, such as that of the simulated dioxane component.

Despite our expectations, the Lorentzian model does not have a clear advantage at lower SNRs, suggesting that the bias in this model is an important factor for all SNRs in the range considered in our study. The results might have been different if, like Webb *et al.* (*8*), we had assumed that all of the NMR parameters except the amplitudes were known from prior information. When such prior information is available, the amplitudes can be estimated at much lower SNRs, and we would expect that the parsimony of the Lorentzian model would be a more substantial advantage.

We evaluated the performance of the AIC, SBC, and HQC methods for selecting the number of knots s by analyzing simulated spin echoes with SNR equal to 100, 30, and 10 using spline models with s = 2, 3, 4, 5, and 6 knots. For each value of the SNR and each of the two parameter sets (based on the analyses of the real MeOH and D10 data sets), we simulated 50 spin-echo data sets. For each simulated data set, the three model-selection criteria were used to choose among the five values of s.

These model-selection criteria are designed to minimize the Kullback–Leibler distance between the fitted and the true models (*13*). In NMR applications, however, we primarily are interested in estimating specific parameters, usually the amplitudes and/or decay rates. Therefore, we evaluated the criteria in terms of their ability to select the model that gave the best estimates of amplitudes and decay rates, not the best model in terms of an overall measure such as Kullback–Leibler distance.

For each simulated data set, we computed the "best" value of s for estimating the amplitude (or decay-rate) parameters, which was defined to be the value that minimized the Ma-

halanobis distance between the true vector of amplitude (decay-rate) parameters and the maximum-likelihood estimate, where the distance was defined in terms of the asymptotic covariance matrix of the maximum-likelihood estimators, assuming the true model from which the data were simulated. We used the covariance matrix for the true model, so that the best estimate was defined without reference to the five Hermitian spline models that were fit to the data. After determining the best estimates and the estimates selected by AIC, SBC, and HQC, we computed the ratio of the mean Mahalanobis distance of the selected estimates to the mean Mahalanobis distance of the best estimates, where the mean was computed over the 50 simulated replications (Table 5). The median of the selected values of s was also computed (Table 6).

The three model-selection criteria were very similar in their performance, with AIC showing a slight tendency, when compared with the other two criteria, to choose models with a greater number of parameters. This property of AIC is well-known (*17*), but AIC seemed to be at no disadvantage in choosing models that give good estimates of the amplitude and decay-rate parameters. The mean distance of the selected estimates from the true values was between 7 and 51% of the mean distance of the best estimates (Table 5).

The median selected value of s, especially when selected by AIC, agreed well with the median of the best values when the best value was selected by the distance of the estimated amplitudes from the true amplitudes. As expected, the selected value of s decreased with the SNR. Surprisingly, the median best value of s, when selected by the distance of the estimated decay rates from the true values, was 3 (except for a value of 2 for the simulated MeOH data at the lowest SNR), regardless of SNR. Closer examination revealed that the error in the decay-rate estimates at SNR = 100 or SNR = 30 is not very sensitive to the choice of s when s = 3, 4, 5, or 6, which also can be seen in the columns labeled "4 knots" and "6 knots" in Tables 3 and 4.

TABLE 5

Results of Simulation Study of Model-Selection Criteria: Ratio of Mean Distance of Selected Estimates to Mean Distance of "Best" Estimates for Simulated Methanol (MeOH) and Water/Dioxane (D10) Data at Three Signal-to-Noise Ratios (SNR)

			Selection criterion		
Parameters	Data	SNR	AIC	SBC	HQC
(α_1, α_2)	MeOH	100	1.07	1.26	1.11
		30	1.29	1.35	1.32
		10	1.27	1.30	1.27
	D10	100	1.11	1.20	1.11
		30	1.47	1.51	1.45
		10	1.21	1.19	1.18
(β_1, β_2)	MeOH	100	1.17	1.17	1.17
		30	1.33	1.32	1.32
		10	1.15	1.16	1.16
	D10	100	1.47	1.47	1.47
		30	1.40	1.40	1.41
		10	1.13	1.15	1.14

TABLE 6

Results of Simulation Study of Model-Selection Criteria: Median Number of Knots (s) in Selected and Best Spline Models for Simulated Methanol (MeOH) and Water/Dioxane (D10) Data at Three Signal-to-Noise Ratios (SNR)

		Selection criterion			"Best" based on	
	SNR	AIC	SBC	HQC	α	β
MeOH	100	6	5	6	6	3
	30	4.5	4	4	5	3
	10	4	3	3	4	2
D10	100	6	6	6	6	3
	30	4	4	4	4	3
	10	3	3	3	4	3

DISCUSSION

We have derived a representation of inhomogeneity distortions as characteristic functions, and we have approximated these distorting functions by a Hermitian regression spline. A comparison of the Hermitian spline and Lorentzian models in applications to phantom and simulated spin-echoes showed that the spline model gave much better fits to the data and better T_2 estimates. Estimation of T_2 from a single spin-echo data set was successfully demonstrated.

The accuracy and precision of single-echo T_2 estimates depends on the following conditions: high SNR; phase cycling to remove artifacts caused by an imperfect refocusing pulse; relatively short T_2 times; and careful measurement of the echo time (τ). Consistently good single-echo T_2 estimates were obtained when the Hermitian spline model with 4 or 6 knots was applied to high SNR data.

Following previous authors (*6–8*), we have assumed that inhomogeneity has the same effect on all spectral components. When this assumption is violated, QUALITY and the method of Webb *et al.* (*8*) will give biased estimates, because both methods assume a single inhomogeneity function computed from a signal or image acquired at the water resonant frequency. In contrast, the Hermitian spline model is easily generalized to handle separate inhomogeneity effects on separate sets of spectral components. As a simple example, suppose that the K components divide into two subsets, indexed by $k = 1, \ldots, K_1$ and $k = K_1 + 1, \ldots, K$, and that all components experience the same inhomogeneity effect

within a subset. Subsets of components can be defined when multiple signal components arise from the same molecule (as in the case of the two components of methanol) and when they are known to arise from two compounds that are well mixed with the same spatial distribution (as in the case of our water and dioxane phantom). Then the Hermitian spline model would have the form

$$Y(t_j) = \psi_1(t_j - \tau) \sum_{k=1}^{K_1} \alpha_k \exp\{-\beta_k t_j + i[\omega_k(t_j - \tau) + \phi_k]\} + \psi_2(t_j - \tau) \sum_{k=K_1+1}^{K} \alpha_k \exp\{-\beta_k t_j + i[\omega_k(t_j - \tau) + \phi_k]\} + N(t_j), \quad [25]$$

where ψ_1 and ψ_2 are approximated by two different Hermitian spline functions.

Inhomogeneity effects are of primary concern in analysis of *in vivo* spectra. While our present model and algorithms may be inadequate for analysis of typical *in vivo* data sets, the spline approach could be combined with sophisticated algorithms such as PIQABLE (*5*), which presently are structured around the Lorentzian model.

ACKNOWLEDGMENTS

The work of Jonathan Raz was supported by National Science Foundation Award DMS-9116730. We gratefully acknowledge the valuable contributions of Donald Twieg, who introduced Dr. Raz to many basic concepts of NMR, and particularly to the problems of modeling spin-echo signals; Robert Sharp, who prepared the phantoms; Andrew Maudsley, Sarah Nelson, and William Redfearn, who made helpful suggestions during development of the methodology; James Pipe, who assisted with data acquisition; and Ronald Thomas and Richard Olshen, who suggested stable distributions.

REFERENCES

1. H. Barkhuijsen, R. de Beer, W. M. M. J. Bovée, and D. van Ormondt, *J. Magn. Reson.* **61,** 465 (1985).
2. J. W. C. van der Veen, R. de Beer, P. R. Luyten, and D. van Ormondt, *Magn. Reson. Med.* **6,** 92 (1988).
3. D. Spielman, P. Webb, and A. Macovski, *J. Magn. Reson.* **79,** 66 (1988).
4. M. I. Miller and A. S. Greene, *J. Magn. Reson.* **83,** 525 (1989).
5. S. J. Nelson and T. R. Brown, *J. Magn. Reson.* **84,** 95 (1989).
6. S. J. Davies, C. Bauer, P. Hore, and R. Freeman, *J. Magn. Reson.* **76,** 476 (1988).
7. A. A. de Graaf, J. E. van Dijk, and W. M. M. J. Bovée, *Magn. Reson. Med.* **13,** 343 (1990).
8. P. Webb, D. Spielman, and A. Macovski, *Magn. Reson. Med.* **23,** 1 (1992).
9. E. Lukacs, "Characteristic Functions," second ed., Griffin, London, 1970.
10. H. Barkhuijsen, R. de Beer, and D. van Ormondt, *J. Magn. Reson.* **67,** 371 (1986).
11. R. L. Eubank, "Spline Smoothing and Nonparametric Regression," Dekker, New York, 1988.
12. G. A. F. Seber and C. J. Wild, "Nonlinear Regression," pp. 657–660, Wiley, New York, 1989.
13. H. Linhart and W. Zucchini, "Model Selection," Wiley, New York, 1986.
14. G. Schwartz, *Ann. Stat.* **6,** 461 (1978).
15. E. J. Hannan, *Statist. Sci.* **2,** 1029 (1987).
16. K. E. Mark and M. I. Miller, *J. Acoust. Soc. Am.* **91,** 989, 1992.
17. M. Davidian and A. R. Gallant, *Biometrika* **80,** 475 (1993).
18. G. H. Golub and C. F. van Loan, "Matrix Computations," second ed., p. 218, The Johns Hopkins Univ. Press, Baltimore, 1989.
19. P. Bloomfield, "Fourier Analysis of Time Series: An Introduction," Wiley, New York, 1976.
20. D. I. Hoult and R. E. Richards, *Proc. R. Soc. London A* **344,** 311 (1975).
21. L. Lin, *Biometrics* **45,** 255 (1989).